Sensors and Actuators B 229 (2016) 63–74

Contents lists available at ScienceDirect

Sensors and Actuators B: Chemical

journal homepage: www.elsevier.com/locate/snb

Improving the performance of electrowetting on dielectric microfluidics using piezoelectric top plate control

Yiyan Li [a,*], R. Jacob Baker [a], Dominic Raad [b]

[a] Department of Electrical and Computer Engineering, University of Nevada, Las Vegas, NV 89154-4026, USA
[b] Kisco Conformal Coating, LLC, San Jose, CA 95119, USA

ARTICLE INFO

Article history:
Received 12 August 2015
Received in revised form
14 November 2015
Accepted 22 January 2016
Available online 25 January 2016

Keywords:
Electrowetting
Digital microfluidics
Gap height
Droplet actuation
Piezoelectric cantilever
Displacement measurement

ABSTRACT

An intelligent EWOD top plate control system is proposed in this study. The dynamic top plate is controlled by a piezoelectric (PZT) cantilever structure. A High resolution laser displacement sensor is used to monitor the deflection of the top plate. The gap height optimization and the top plate vibration significantly improve the droplet velocity and decrease the droplet minimum threshold actuation voltage. The top plate vibration induced actuation velocity improvement is magnitude and frequency dependent. 100 μm and 200 μm vibrations are tested at 25 Hz. Vibration frequencies at 5 Hz, 10 Hz, and 20 Hz are tested while the magnitude is 200 μm. Results show greater improvements are achieved at larger vibration magnitudes and higher vibration frequencies. With a vibrated top plate, the largest reduction of the actuation voltage is 76 V_{RMS} for a 2.0 μl DI water droplet. The maximum droplet instantaneous velocity is around 9.3 mm/s, which is almost 3 times faster than the droplet velocity without top plate vibration under insufficient driving voltages. Liquid that has different hysteresis such as acetonitrile with various concentrations are used as a control to show its compatibility with the proposed DMF chip. Contact line depinning under top plate vibration is observed, which indicates the underlying mechanism for the improvements in actuation velocity and threshold voltage. The top plate control technique reported in this study makes EWOD DMF chips more reliable when used for the clinical point-of-care diagnostic applications.

1. Introduction

Electrowetting on dielectric (EWOD) digital microfluidics (DMF) is one of the most promising lab-on-a-chip techniques [1]. With friendly interfaces to computers and microcontrollers, batch processing of droplet actuation [2], merging [3], splitting [4], position detection [5–7], droplet composition identification [8,9] and even volume controlled dispensing are all possible on a DMF chip [6,10]. EWOD DMF chips can be fabricated on low-cost substrates such as glass [11,12], printed circuit board (PCB) [10,13–15], polyimide film [16] and paper [17]. As the cost and size of the DMF chip decreases, the EWOD system can be integrated with portable electronics for point-of-care diagnostics [11,12,18]. Generally, a robust and clinically practical DMF device should have properties such as disposable DMF electrode card, efficient droplet actuation, low actuation threshold voltage, and high dielectric break down voltage.

Efforts have been made to lower the threshold voltage and speed-up droplet actuation. These efforts include reducing the liquid-dielectric interfacial tension [19], using the materials that have larger dielectric constant [19,20], using an oil environment [19–24] and decreasing the dielectric insulator thickness [19,20]. However, using an oil environment may contaminate the diagnostic chemicals; thinner dielectric layers are vulnerable to pinholes and dielectric break down. The droplet actuation velocity is mainly dependent on the roughness of the hydrophobic surface, the composition of the droplet, and the strength of the electric field. The droplet actuation velocity can be improved by using a single-plate topology to avoid the extra friction from the top plate [25]. Also, it can be improved using a silicone oil environment in a chamber to eliminate the contact angle hysteresis [26]. Additionally, modulating the driving voltages are reported to increase the actuation velocity such as using a single pulse [27], pulse train [28], AC waves [14] and pulse-width modified voltages [29–31].

* Corresponding author.
E-mail addresses: liy10@unlv.nevada.edu, ianleevlsi@gmail.com (Y. Li), r.jacob.baker@unlv.edu (R.J. Baker), draad@kiscoparylene.com (D. Raad).

http://dx.doi.org/10.1016/j.snb.2016.01.108
0925-4005/

The top plate introduces more frictions and therefore requires a higher actuation threshold voltage. Another uncertainty introduced by the top plate is the aspect ratio [32], which is the ratio of the gap height to the droplet pitch. The aspect ratio has been reported in its significant influence on droplet kinetics [33,34]. Homogeneous gap height cannot provide optimized droplet operation if the droplets have various volumes. Conventionally, a double sided tape is used as the spacer for the dual-plate configuration [11,12,35]. The thickness of a layer of the standard commercially available double sided tape is roughly 50–75 μm. Adjusting the gap height by adding or removing the tape layers is too coarse for optimizing the system's performance. Thus, a continuously adjustable gap height is desired. So far the finest gap height control using a DC motor [33] suffers from a limited resolution (50 μm). In this study, the traditional DMF system is optimized using a quasi-static top plate to accurately adjusting the gap height and gently adding top plate vibrations. A precise top plate positioning technique is achieved by using two bimorph piezoelectric (PZT) cantilever beams. A cantilever beam is a rigid structure which has only one end anchored and another end is used to support the load. Cantilever structures can be found in both large constructions (such as bridges, buildings and aircrafts) [36,37] and small microelectromechanical systems (MEMS) [38,39]. The PZT plate can resolve sub-micron displacements. Piezoelectric actuators are widely used for accurate positioning tasks [40,41]. Controlled by the PZT actuator, the top plate can be precisely positioned and vibrated.

For more than 100 years, scientists have been fascinated with vibration induced droplet motions [42,43]. Vertical and horizontal harmonic vibration of the supporter can break the balance of the droplet and induce a liquid movement. The oscillating magnitude, frequency and phase dominate the vibration induced behaviors [42]. Different from the external substrate vibration, more powerful internal droplet oscillations can be created by surface acoustic waves (SAWs) [44–51]. However, the major concerns of using SAWs as actuators are the unpredictable rapid fluid flow and integration issues of the vibration source with the silicon and glass substrates in EWOD [52]. Substrate vibration was used to actuate a droplet on a surface with chemically wettability gradient [53]. A promoted droplet motion on a chemical gradient surface is realized by controlling a sandwiched structure which is similar to the popular DMF topology. In Daniel's study, a droplet ratchet-like motion is observed by continuously squeezing and relaxing the droplet. The contact line was depinned during the vibration and moves to the surface with lower interfacial energy. In electrowetting, a double layer of charges near the liquid-solid surface is formed by the electric field applied to the electrode [54]. The charge double layer lowers the surface energy which helps spread the liquid on the surface. Therefore, it is possible to use top plate vibration to overcome the surface hysteresis and lower the actuation voltage.

In this study, a PZT controlled DMF top plate is used to accurately define the gap height and provide vibrations to optimize the droplet operations on the proposed DMF system. The droplet actuation threshold voltage and velocity are tested with various top plate heights and top plate vibration magnitudes and frequencies.

2. Materials and methods

2.1. System design

Precise gap height control can be realized using two PZT cantilever beams. The EWOD chip (37.5 mm × 37.5 mm with 27 electrodes) is fixed on a PCB platform (Fig. 1(a) and (b)). The top plate is mounted to two PZT plates which are fixed by two binding posts. The on-chip chromium pins are connected to stranded wires using silver conductive epoxy. The top plate ITO (indium-tin-oxide) layer is grounded all the time for proper droplet operations. A high voltage module purchased from EMCO (EMCO F40, Schweiz, Switzerland) is used as the high voltage source to provide the driving voltages to the PZT chip and the EWOD electrodes. The great benefit of using EMCO and the simple CMOS gate arrays as the EWOD driving circuit is saving the space of using bench function generators & amplifiers. Laser displacement sensor (Z4M-S40, Kyoto, Japan) and its manufactural amplifier (Z4M-W40, Kyoto, Japan) are used to monitor the PZT displacement. The laser displacement sensor can perform high resolution (100 nm), broad bandwidth (1 kHz) and contactless displacement measurement. Fast and precise displacement data can be acquired without affecting the mechanical vibration properties of the structure. The output voltage from Z4M-W40 is 0–200 mV, a second stage amplifier is required to levitate the voltage level for the ADC (ADC, 0-3.3 V) (Fig. 1(c)). A desktop PC (ASUS, Intel i5 2.53 GHz, RAM 8 GB) is used for data collection and sending feedback driving voltages to the DAC & MCU module. The DAC translates the digital driving voltages to 0–2.54 V. An additional linear DC high voltage amplifier is developed to modulate the 0–2.54 V to 0–200 V to drive the PZT plates. The feedback loop can be automatically controlled by the software built in the PC, or visually controlled by a person if needed.

A novel modular design is introduced to the EWOD system. The EWOD electrode control system is integrated into two portable modules (Fig. 1(b)); one is the relay array, the other one is the control hub. The EWOD chip is mounted on a PCB platform and connected to the relay array module with standard flexible flat cables (FFC). EWOD electrode driving voltages are obtained from the drains of the high-voltage CMOS transistors (Fig. 1(d)). Various frequencies of the actuating voltage can be obtained by toggling the gates of the transistors with different rates [5,8,13] (DC pulses at 10 kHz and various voltages).

2.2. The DMF EWOD chip fabrication

Devices were fabricated in the cleanroom facility of Nevada Nanotechnology Center at University of Nevada, Las Vegas. The fabrication reagents includes Schott Boro Float glass substrate with Chrome coated (100 nm) microfluidic blank slides (with positive photoresist coated, Telic, Valencia, CA, USA), Teflon-AF solution (amorphous fluoroplastic resin in solution, 400S2-100-1, DuPont, Mississauga, ON, CA), photoresist developer RD6 (Futurrex, INC., Franklin, NJ, USA), Chromium etchant (Sigma-Aldrich, Co., MO, USA), photoresist remover (Microposit Remover 1165, Rohm and Haas Electronic Materials LLC, MA, USA), indium tin oxide (ITO) coated glass (Adafruit INC., NYC, USA). Open source integrated circuit (IC) layout tools Electric VLSI [55] is used to pattern the mask of the electrode array. GDSII output files from Electric VLSI are sent to Infinite Graphics INC. (MN, USA) for plotting (25,000 dpi). During the photolithography process, the substrates are covered by the patterned photomask and exposed to a UV light source for 45 s and then developed for 1 min in RD6. Substrates are then immersed in the Chromium etchant for about 15–20 s. Then the substrates are washed by DI water and dried out using nitrogen gas. The remaining photoresist is removed by Microposit Remover 1165.

It is more challenging to realize the droplet actuation, merging and splitting in an air environment rather than in an oil environment. The oil environment in the EWOD chip, to some extent, is more tolerant to dust. Also, without an oil environment, the two major microfluidic kinetic resists, the contact line pinning and contact angle hysteresis (CAH), become much more significant to prevent the droplet from being actuated. To realize a smooth actuation in air, larger electrostatic force is required. A morphological representation of the electrostatic force is the contact angle change. Obviously, the driving voltage has to be limited within the dielectric material break down voltage. Among all the candidate insulator

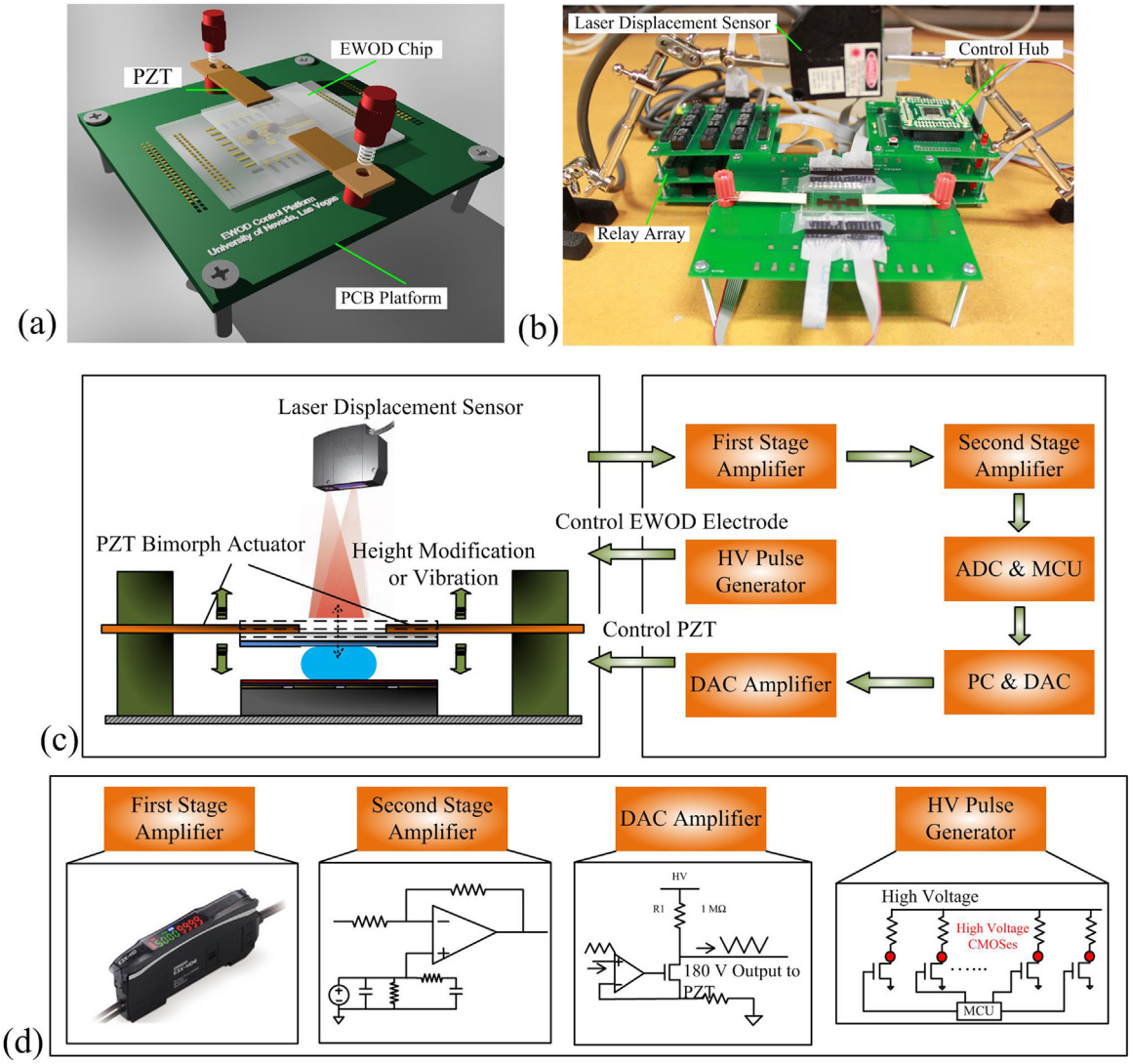

Fig. 1. (a and b) The 3D model and the experiment setup of the EWOD platform. (c and d) The system overview of the DMF and the PZT top plate control module.

materials, parylene C stands out for its high dielectric constant and the high break down voltage. In order to make the surface more robust for higher voltages, an 8 μm parylene C is coated to the EWOD chip by a chemical adhesion process. Prior to parylene C coating, the chips were cleaned using a Plasma Etch process. The Plasma etch process utilizes Oxygen and an inert gas (Argon or Nitrogen) to increase surface wettability and remove any oils or fiber-molecules. Then, the chips are fixed on the masked areas. The chips are loaded into the CVD chambers. Vapor-Phase Silane (VPS) is introduced into the chamber and acts as an aerosol primer to enhance the chemical adhesion to the parylene C surface. The parylene dimer is loaded into the pyrolizer and enters the chamber with the EWOD chips as a monomer gas. The gas polymerizes on any surface area that remains at room-temperature. The gas flow is manipulated and deposit in such a way that the thickness and the uniformity of the coating can be controlled. 250 nm Teflon AF solutions are then spin coated on the chip as the hydrophobic top layer.

2.3. Actuation velocity and minimum actuation voltage measurement

A high speed camera (up to 1000 fps, Casio ZR200, Japan) and a handled digital microscope (Celestron, CA) are used to capture the droplet motion and measure the instantaneous velocity. The actuation velocity and the minimum threshold voltage depend on the droplet volume, top plate height, top plate vibration magnitude and frequency. The top plate height and vibration are controlled by the commands sent from the PC. Feedback signals of the real top plate height are displayed on the PC monitor in real time so the top plate can be adjusted to the desired height by adjusting the PZT driving voltages. Open source software ImageJ and Tracker are used to measure the droplet displacement and volumes.

The droplet driving voltage is controlled by a potentiometer and monitored by an oscilloscope. The minimum threshold voltage is recorded as the minimum voltage to actuate the droplet. The driving voltages are recorded as an average of six repeated tests. To avoid the voltage and velocity deviations caused by different electrodes, the minimum actuation voltage and the maximum

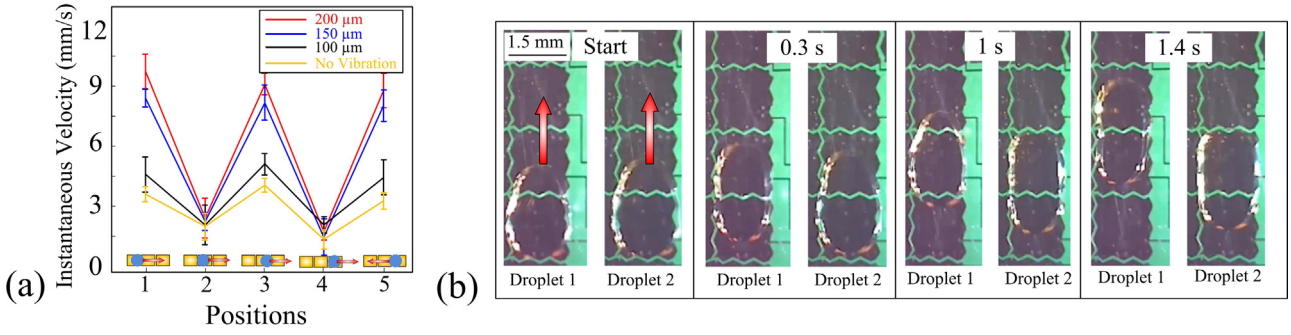

Fig. 2. Top plate vibrations speed up the droplet velocity. (a) Droplet instantaneous velocity at five different positions while the droplet travels through three electrodes. (b) Consecutive snapshots of water droplets with 200 μm (Droplet 1) and 100 μm (Droplet 2) top plate vibrations. (A short video is available for this experiment: Vibration Speed Up_01).

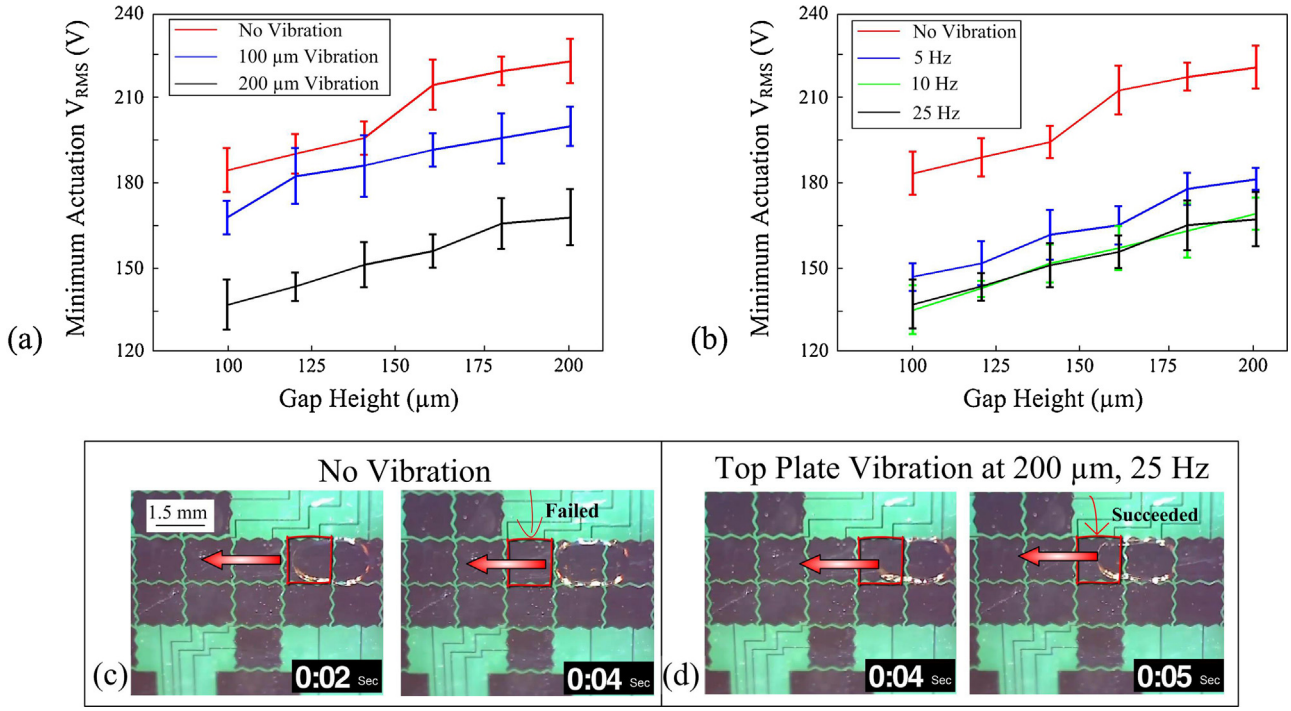

Fig. 3. Comparison of the minimum actuation voltages of a droplet (2.0 μl) under various top plate vibration magnitudes (a) and frequencies (b). (c) Consecutive snapshots of a failed actuation without top plate vibration and (d) a succeeded actuation with a 200 μm, 25 Hz vibration under the same driving voltage. (Supplementary material is available: Contact Line Pinning Cancellation_02).

instantaneous velocity are measured with the same starting electrode and target electrode. The droplet velocity is analyzed using Camtasia (Okemos, MI) ($dv = ds/dt$, v is the velocity, s is the displacement, t is the time spent for the movement).

3. Results and discussions

3.1. DMF optimization by top plate vibration

In this study, it is assumed that vibrating the top plate instead of vibrating the substrate can lower the actuation threshold voltage, release the pinned droplet, and decrease the failure rate of the experiments. This gentle intervention added to the EWOD system will not harm normal EWOD operations. Here, PZT bimorph piezoelectric plates are employed as the vibration source for the top plates. The PZT chip displacement and vibration behavior have been extensively studied [41,56,57]. Sub-milimeter vibration can be well controlled by a computer system, which makes it a perfect candidate to be the EWOD top plate holder and actuator.

In Fig. 2, the subfigures are consecutive snapshots of the droplet actuation with top plate vibration at 200 μm and 25 Hz (Droplet 1) and 100 μm, 25 Hz (Droplet 2). The vibration baseline is at 100 μm away from the bottom plate; the vibration goes from "100 μm + *0* μm" to "100 μm + *100 μm*" or "100 μm + *200* μm" but never goes below the baseline (100 μm). The droplet under stronger top plate vibration has a significantly higher instantaneous velocity while the droplet travels through the three electrodes (Fig. 2(a)). At 220 V_{RMS}, the maximum droplet instantaneous velocity is around 9.3 mm/s which is almost 3 times faster than the droplet velocity without top plate vibration (Fig. 2, a short video is available for this experiment: Vibration Speed Up_01). The droplet velocity improvements are more significant under stronger top plate vibrations.

The vibration magnitude dependent actuation enhancement is investigated (Fig. 3). The minimum actuation voltage is the threshold voltage to trigger the droplet to move. First, a droplet was dispensed from the reservoir at a certain gap height. The droplet driving voltage was adjusted using a potentiometer. To avoid the

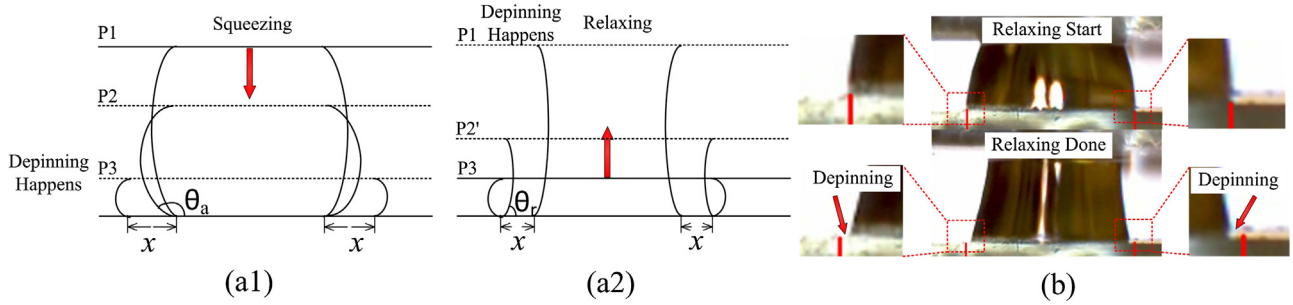

Fig. 4. A cross-sectional view of a DI water droplet that is sandwiched in a DMF system with a 5 Hz, 200 μm top plate vibration (no voltage is applied to the electrode). (a1) Squeezing a droplet and the depinning happens at P3. (a2) Relaxing a droplet and the depinning happens at P1. In (a1–a2), droplet contact line moves a distance of "*x*" along the surface. (b) Experiment shows the contact line depins when relaxing the water droplet.

deviations caused by different electrodes, the minimum actuation voltage is measured with the same starting electrode and destination electrode for six times. The six tests were conducted continuously with the same vibration magnitude and the same droplet position. Using low driving voltages around threshold voltage can activate the droplet but the movement is not smooth and prone to contact line pinning. Top plate vibration can overcome the contact line pinning issue while using low driving voltages. If the top plate vibration can expedite the droplets at lower driving voltages, the threshold voltage is reduced by the vibration. No top plate vibration and 200 μm top plate vibration are tested (Fig. 3(c) and (d)). A failed actuation is observed (Fig. 3c at 0:04 s, supplementary material is available: Contact Line Pinning Cancellation_02). While in Fig. 3(d), the droplet is activated and smoothly transported to the target electrode at 205 V_{RMS}. The contact line pinning is eliminated by the top plate vibration.

For a better understanding of the underlying mechanism for the velocity and threshold voltage improvements, the droplet contact line dynamics are analyzed by observing the cross-sectional view of the droplet under top plate vibrations (Fig. 4, no voltage applied). The liquid-solid contact angle changes with top plate vibrations due to the continuous squeezing and relaxing operations of the droplet even when there is no voltage applied (Fig. 4). When squeezing the droplet, the contact line is pinning at the same location with an increasing contact angle until it reaches the advancing angle θ_a (Fig. 4(a1)); when relaxing the droplet, the contact line keeps pinning at the same location until the contact angle reaches the receding angle θ_r (Fig. 4(a2)). Therefore, a strong enough top plate vibration that induces sufficient contact angle changes can depin the contact line. A sequential squeezing and relaxing operation allows the droplets to experience various metastable states that results in easier actuation toward the minimum global energy [53,58]. Once an asymmetrical voltage gradient is applied to the surface, the droplet contact angle at the higher voltage side drops substantially which results in an unbalanced electrostatic force that drags the droplet forward.

Low frequency top plate vibration (<25 Hz) depins the droplet contact line and makes the droplet actuation easier. One typical study using bottom substrate vibrations (30–1100 Hz) found 37 resonance modes of sessile droplets [59]. The droplet vibration patterns are observed indirectly through analyzing the deformation of a meshed background [59]. In this study, we use top plate vibration instead of using substrate vibration for the EWOD device. The top plate vibration platform can be developed with mounted PZT chips which are friendly to external electronics. However, the disadvantage of this PZT is its limited bandwidth. In order to overcome the contact angle hysteresis for the actuation, the vibration magnitude has to be "large" enough (> 100 μm). The PZT chip vibration magnitude attenuates significantly at high frequencies. According to the studies in the bottom plate vibration [53], significant velocity amplification was observed when the substrate vibration matched the natural harmonics of the drop oscillation. However, the natural harmonic oscillation of the droplet in micro liter level is usually > 300 Hz (varies with droplet mass). The PZT chip used in this study has a manufactural bandwidth of 200 Hz which is much smaller than the droplet's natural oscillation harmonics (the bandwidth goes even smaller when the PZT is loaded with the top plate).

The target electrode is applied with a voltage that changes the wettability of the surface, which is known as "electrowetting". It was first identified by Greenspan [60] that a liquid droplet placed on a chemically heterogeneous surface moves to the region of higher wettability to reduce the interfacial free energy, and experimentally demonstrated by Daniel [53,61] on a vibrated substrate with a chemical wettability gradient. It was reported that low frequency bottom substrate vibration (1 Hz) induced a droplet ratchet-like motion toward the more wettable region because of the successive pinning and depinning of contact lines allows the drop to sample various metastable states and thereby setting it to the path of global energy minima [53]. Similarly, "electrowetting" modifies the wettability of the surface with a voltage gradient instead of using a chemical gradient. If the voltage gradient is weak (low voltages), the actuation would not happen. The "top plate vibration" used in this study can trigger the droplet actuation even with a weak voltage (Fig. 5, using a 3 μl water droplet for a good observation of the contact angles). The voltage gradient on the DMF chip developed in this study is a binary form which has only the voltage "on" and voltage "off" status (wetting and de-wetting). The liquid that bridges both the "on" and the "off" electrodes has an asymmetrical contact angle hysteresis (Fig. 5). θ_{aL}, θ_{rL}, θ_{aR}, and θ_{rR} are the left advancing angle, the left receding angle, the right advancing angle, and the right receding angle. In Fig. 5, $\theta_{aL} > \theta_{aR}$, when squeezing the droplet, the right contact angle reaches θ_{aR} earlier and moves to the right before the left contact angle reaches θ_{aL}, which causes the left contact line to stay at the same location while the right contact line moves; when relaxing the droplet ($\theta_{rL} > \theta_{rR}$), the left contact angle reaches θ_{rL} earlier and moves to the right before the right contact line can get a chance to recede (Fig. 5(c)). The asynchronous contact line movement on the left and the right side of the droplet forges a ratchet-like motion which overcomes the contact angle hysteresis on the liquid-solid interface. This enables the liquid to move under lower voltages or move quicker with a normal driving voltage.

In Electrowetting, a double layer of charges near the liquid-solid surface is formed by the electric field applied to the electrode [54]. The charge double layer lowers the surface energy, which helps spread the liquid on the surface. When the right contact line is depinned by squeezing the droplet, not only the right contact line moves but the left contact line also gets a small displacement ("d1"

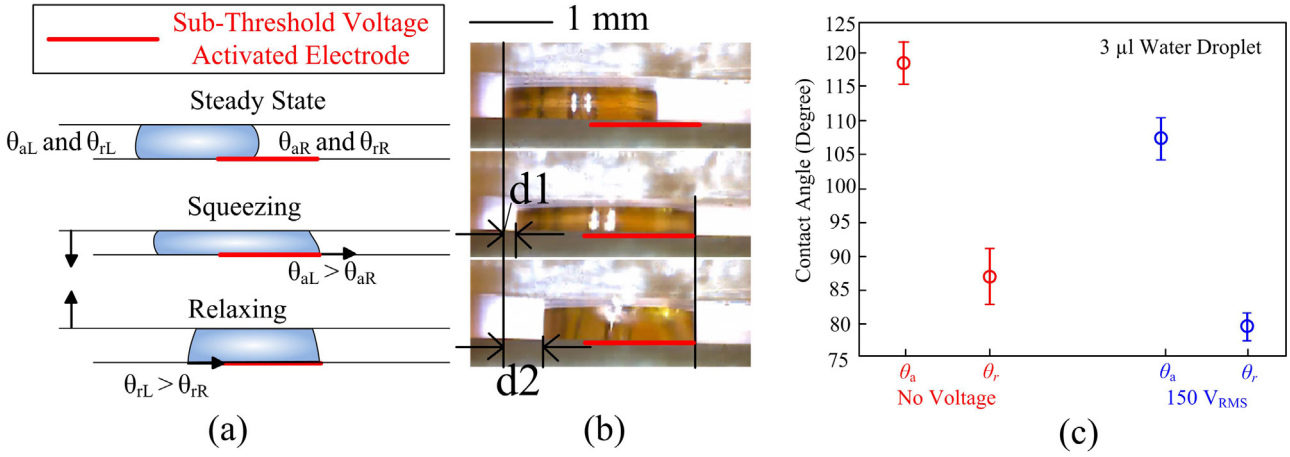

Fig. 5. (a) θ_{aL}, θ_{rL}, θ_{aR} and θ_{rR} are the left advancing angle, the left receding angle, the right advancing angle, and the right receding angle. The voltage applied to the electrode (using 150 V_{RMS} here) is lower than the actuation threshold voltage. The droplet has an asymmetrical contact angle hysteresis at the left and the right contact line. Because $\theta_{aL} > \theta_{aR}$, when squeezing the droplet, the right contact angle reaches θ_{aR} earlier and moves to the right before the left contact angle reaches θ_{aL}; similarly, $\theta_{rL} > \theta_{rR}$, when relaxing the droplet, the left contact angle reaches θ_{rL} earlier and moves to the right before the right contact line can get a chance to recede. (b) Top plate vibration triggers a ratchet-like movement of a 3 µl water drop under sub-threshold actuation voltages. (c) The advancing and receding contact angles with no voltage and with a subthreshold voltage (150 V_{RMS}) applied.

in Fig. 5(b)), which manifests a stronger force than the chemical gradient can provide that propels the droplet forward.

Acetonitrile, which is well-known for its low viscosity (0.37 m^2/s) and negligible contact angle hysteresis, is used as a control for the droplet velocity test under top plate vibrations. If the contact angle hysteresis is small, $\theta_a \approx \theta_r$, the vibration will not add any displacement to the droplet as indicated by the following equation [53]:

$$x = \frac{\alpha V^*}{4\omega}\left[\left(\cos\theta_{rR} + \cos\theta_{aR}\right) - \left(\cos\theta_{rL} + \cos\theta_{aL}\right)\right] \quad (1)$$

in which x is the droplet displacement, $V^* = \gamma/\eta$, γ and η are the surface tension and the viscosity of the drop. If the contact angle hysteresis is negligible, $\left(\cos\theta_{rR} + \cos\theta_{aR}\right) - \left(\cos\theta_{rL} + \cos\theta_{aL}\right) \approx 0$. Our experiment shows droplets with a high concentration of acetonitrile is very difficult to be moved on the EWOD surface with normal actuating voltages (>250 V_{RMS}), even there is a top plate vibration. The contact angle change is very small for high concentrated acetonitrile (Fig. 6), which indicates a weak electrostatic force. A pure acetonitrile droplet is not moveable in an EWOD DMF device. Only aqueous solutions of acetonitrile with low concentrations (<25%) are movable.

However, for a sessile water droplet, the droplet-substrate contact angle varies with the electrowetting number (η):

$$\cos\theta = \cos\theta_Y + \frac{\varepsilon_0\varepsilon_d}{2d\sigma_{lv}}U^2 = \cos\theta_Y + \eta \quad (2)$$

in which θ_Y is Young's equilibrium contact angle, ε_d is the dielectric constant of the insulation layer, d is the thickness of the insulation layer, σ_{lv} is the liquid-vapor surface tension, U is the applied voltage. When the applied voltage increases, the contact angle decreases very quickly until it is saturated. The electrowetting property of a sessile droplet is shown in Fig. 7 (for typical values: $\sigma_{lv} = 0.072\,J\,m^{-2}$ and the dielectric material layer thickness is $d = 8\,\mu m$).

The decreasing rate of the contact angle (Fig. 7(b)) slows down when the driving voltage is larger than 250 V_{RMS}. This indicates the contact angle is getting saturated at higher voltages.

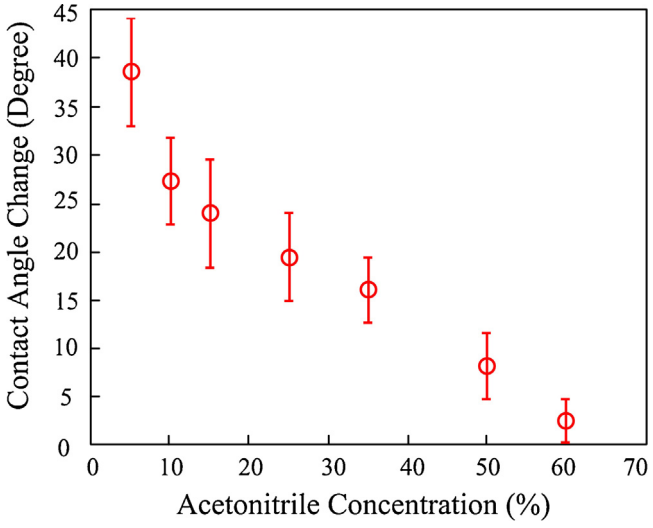

Fig. 6. Contact angle changes of a 3 µl acetonitrile droplet with varying concentrations. 250 V_{RMS} pulses are applied to the electrode.

3.2. DMF optimization by changing the gap height

3.2.1. Lowering the minimum actuation voltage and speed up the droplet actuation

The purpose of the gap height optimization is to decrease the minimum actuation voltage and increase the actuation velocity. The droplet footprint area and volume have great influences on the actuation efficiency. The relationship of footprint area A, droplet volume V and gap height H can be estimated using the following equations:

$$V = A \times H \quad (3)$$

With the same droplet volume, the droplet footprint area can be controlled by adjusting the gap height. The droplet volume varies due to unequal dispensing, splitting or evaporation. The gap height should be adjusted to keep good footprint area for a smooth actuation. The relationship between the minimum threshold voltage and

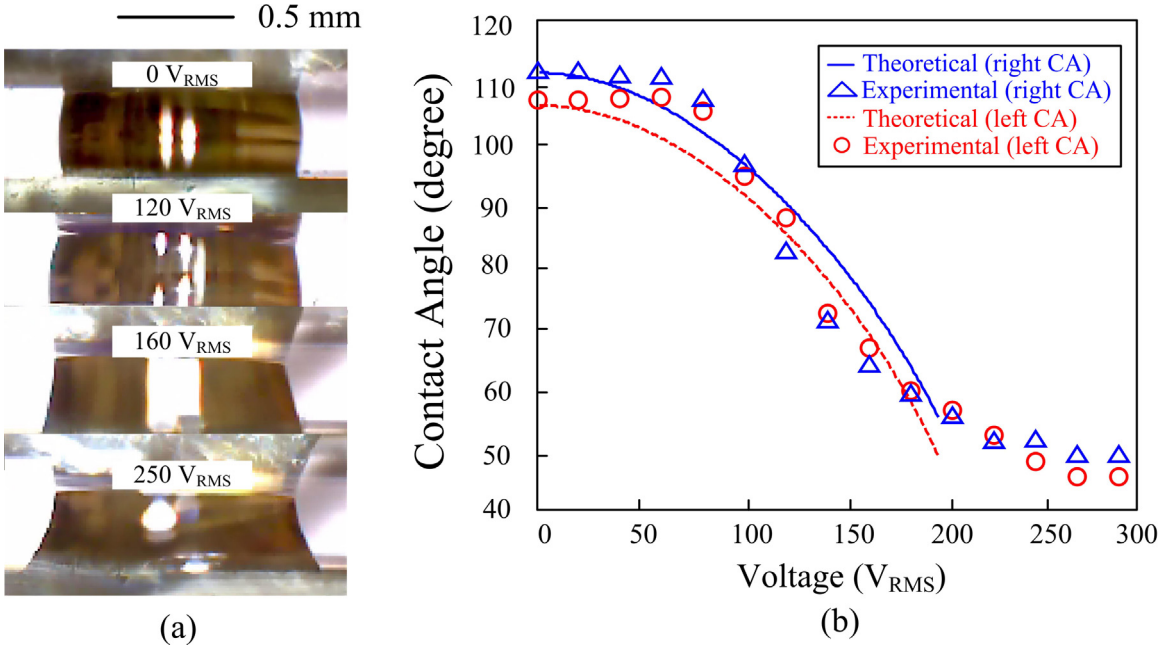

Fig. 7. (a) Contact angle versus applied voltage (V_{RMS}) for a DI water droplet that sandwiched between two Teflon (250 nm) coated substrates in an air ambient. (b) Experimental and theoretical contact angle changes of both the left and the right side of droplet.

the gap height can be represented by the following equation [34]:

$$V_{\min} = \left[\left(\frac{\varepsilon_0 w}{4d_2\Upsilon} \times \frac{1}{\frac{d_1}{\varepsilon_T} + \frac{d_2}{|\varepsilon_w^*|} + \frac{d_3}{\varepsilon_T} + \frac{d_1}{\varepsilon_T}} - \frac{1}{\frac{d_1}{\varepsilon_T} + \frac{d_2}{1} + \frac{d_3}{\varepsilon_p} + \frac{d_1}{\varepsilon_T}}\right)\right]^{-1/2} \quad (4)$$

and

$$\varepsilon_w^* = \varepsilon_w - j\frac{\sigma}{2\pi f\varepsilon_0} \quad (5)$$

where ε_0, ε_T, ε_p and ε_w^* represent the permittivity of vacuum, Teflon, parylene C and water. d_1, d_2, d_3 are the thickness of the Teflon, gap and parylene C. w is the width of the electrode. γ is the surface tension [34]. σ is the fluid conductivity of water. The relationship between the gap height and the minimum actuation threshold voltage can be approximated. However, in the real experiments, the diagram of the voltage and the gap height won't be monolithic (as shown in Eq. (4)). If the top plate height is too low, the droplet is squashed to a random shape; the applied electrostatic force will not provide enough power for the actuation before the contact angle gets saturated.

Except for the gap height, there are several other environmental factors which will affect the minimum actuation voltage; such as the droplet volume, the footprint area, the droplet aspect ratio and the roughness of the surface. The minimum threshold voltage was tested with varying droplet volumes and gap heights in this study. Droplet volumes from 0.2 μl to 2.0 μl, gap heights from 50 μm to 200 μm are tested for the minimum actuation voltage.

The color-map shown in Fig. 8 is a 7 by 7 matrix, which has 49 points in total. There are 7 different heights and volumes. The color-map using discrete colorful boxes shows the original data.

The blue boxes in Fig. 8(a) show the optimized gap heights for the droplets in 0.2–0.8 μl. The minimum actuation voltage overall is 144.9 V_{RMS} (50% duty cycle high frequency pulses are converted to RMS values) which occurs at 0.2 μl and 50 μm gap height. The droplets' volume ranges from 0.5 μl to 2.0 μl are more flexible to various gap heights. Large droplets with high gap heights have larger minimum actuation voltage. Droplets with volumes less than 0.8 μl are easier to be actuated (Fig. 8(a)). The droplet maximum instantaneous velocity shows the fastest moment that the droplet travels through three continuous electrodes. Most of the fastest droplets are the ones that are close to the diagonal of the color-map in Fig. 8(b). While the droplet has a size of 0.6–1.7 μl, the gap height should between 100 and 170 μm.

3.2.2. *Droplet dispensing volume control and dispensing voltage optimization*

A smaller working droplet is generated from a larger electrode (reservior). The forwarding electrode should be activated first to drag a certain amount of liquid from the reservoir. The electrodes in the middle of the reservoir and the targeting electrode are turned off to disconnect the dispensed droplet from the reservoir (Fig. 9). The biggest issue of EWOD dispensing is the volume control. It is hard to control the dispensed droplet volume accurately. Adding capacitive sensors to a feedback control loop to manipulate the dispensed droplet volume in real time can improve the volume accuracy [10]. But the droplet-electrode capacitive data is influenced by the droplet position as well [8].

A fast and accurate EWOD dispensing volume control method is proposed in this study. Once the size of the reservoir and the working electrodes are known, the dispensing droplet volume can be modified by changing the gap height. A high resolution gap height control method is desired for this modification. The gap height and the dispensed droplet volume look-up table can be obtained experimentally. Then setup of a proper gap height during the dispensing process is possible to generate a droplet with a certain volume (Fig. 9, A movie is available in the supplementary materials: Dispensing Volume Control-03).

For the maximum instantaneous velocity shown in Fig. 9(b), the droplet movement from one electrode to another electrode is an accelerating motion at the beginning followed by a decelerating movement. The six tests were conducted continuously with the same gap height and the same droplet position. For the threshold voltage, the SD ranges from ±1.7 V to ±8.6 V, the maximum velocity SD ranges from 0.05 mm/s to 0.37 mm/s.

As shown in Fig. 9, the theoretical dispensed droplet pitch is close to the droplet length (width). However, the experimental droplet pitch and footprint area is measured using ImageJ. The

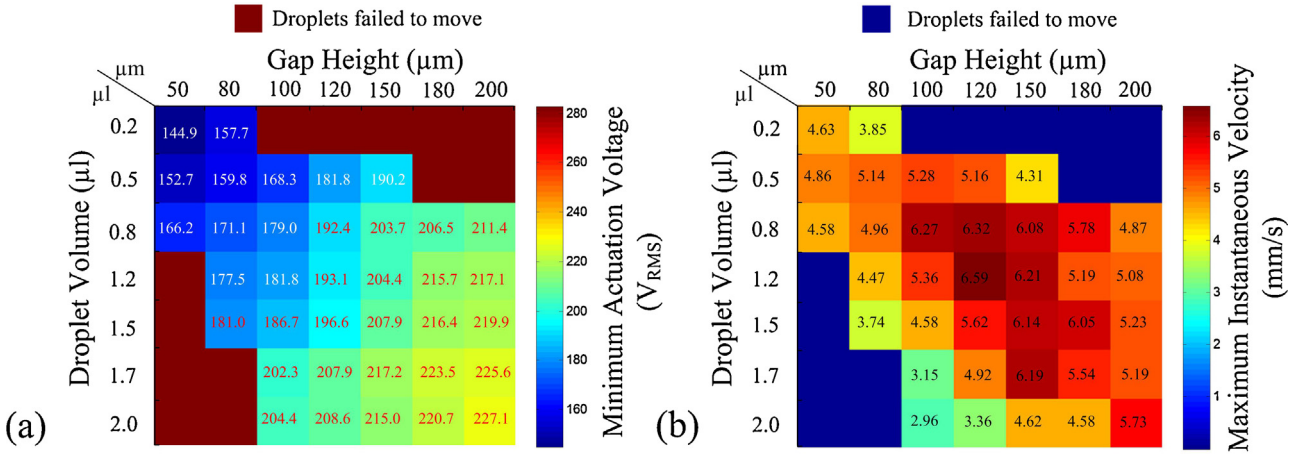

Fig. 8. (a) The map of the minimum actuation voltage for various gap heights and droplet volumes and (b) maximum instantaneous droplet velocity with various gap heights and droplet volumes (at 300 V_{RMS} and 10 kHz).

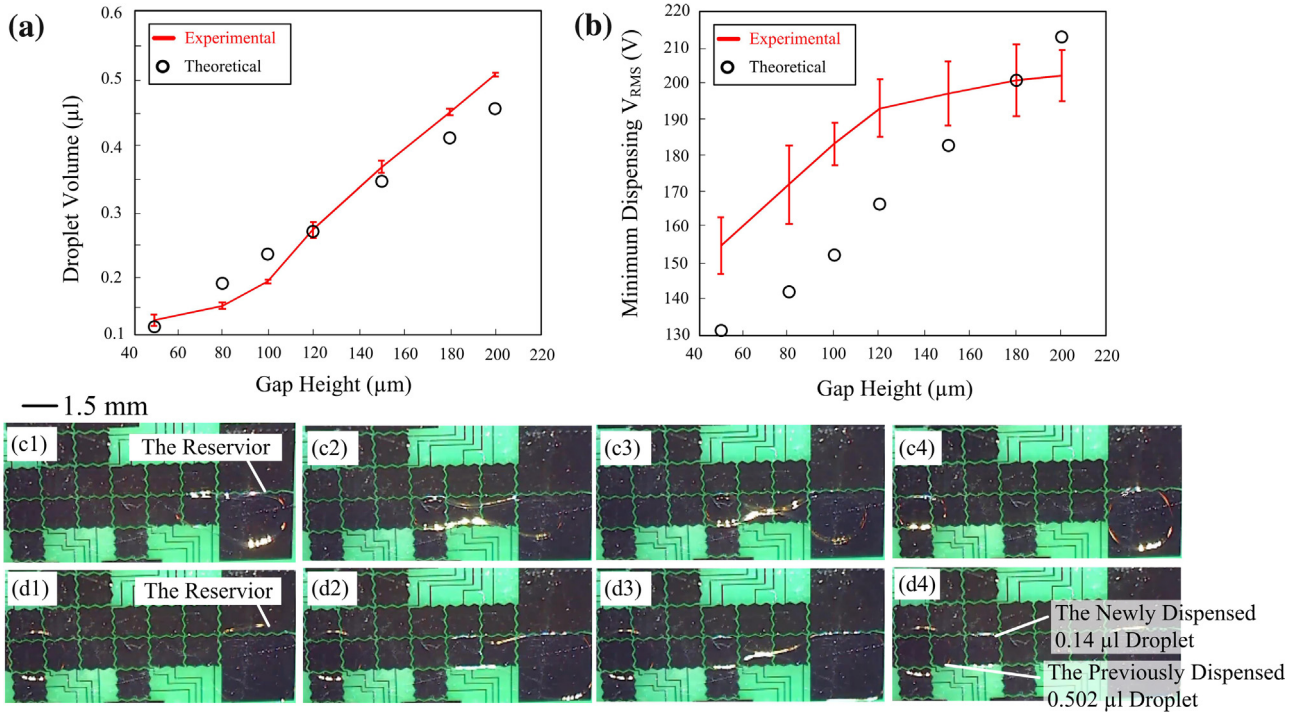

Fig. 9. (a) The relationship between the gap height and the dispensed droplet volumes. (b) The minimum dispensing voltage increases as the gap height increases. (c1–c4) Dispensing a 0.502 μl droplet at the gap height of 200 μm. (d1–d4) Dispensing a 0.14 μl droplet at the gap height of 75 μm.

differences between the theoretical approximation and the experimental measurement are compared in Fig. 9(a).

All the dispensing operations at the same top plate height were conducted six times. The theoretical dispensed droplet volume is calculated by assuming that the footprint area is the same as the electrode area (explained in Fig. 10), which is 1.5 mm × 1.5 mm = 2.25 mm^2. The theoretical dispensed droplet volume can be calculated as: $V = A \times H$ (if there is a voltage applied to the rectangular electrode, when the droplet pitch is much larger than the gap height, the droplet topology is close to a cuboid). V is the droplet volume, A is the electrode area which is a constant in this case, H is the gap height. For example, a 0.1 μl droplet can be dispensed with a gap height of 50 μm (2.25 mm^2 × 50 μm = 0.112 μl ≈ 0.1 μl).

The theoretical dispensing voltage is a little bit smaller than the splitting voltage but larger than the threshold voltage. The minimum dispensing voltage can be calculated by Eq. (6) [62],

$$V = \sqrt{\frac{8\gamma_{lg} \times t \times d}{L \times \varepsilon_0 \times \varepsilon_r \times \left(N^2 + 1\right)} + V_T^2} \tag{6}$$

in which V is the minimum dispensing voltage, γ_{lg} is the liquid-substrate interfacial tension, t is the dielectric layer thickness, d is the gap height, L is the electrode pitch, ε_0 is the vacuum permittivity, ε_r is the dielectric coating permittivity, N is the electrodes engaged in dispensing the droplet, V_T is the threshold voltage for

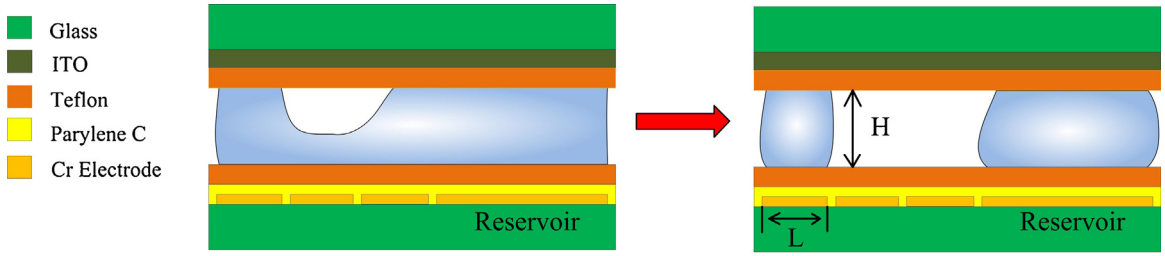

Fig. 10. The pitch of a dispensed droplet is similar to the electrode length L (and width).

droplet actuation. The theoretical and experimental minimum dispensing voltages are shown in Fig. 9(b).

The deviations of the experimental data to the theoretical data in Fig. 9(b) are caused by the following reasons: (1) the two variables, d and V_T, in Eq. (6) are obtained experimentally. Measurement errors caused by frictions, contact angle hysteresis and shear force were not considered in this equation; on the other hand, the contact angle hysteresis affects the reproducibility of the experimental dispensing voltages. From Fig. 9(b), the experimental dispensing voltages increase with increasing gap height, the SD of dispensing voltages for each gap height ranges from 6 V to 11 V. We can also notice that the slope of the experimental minimum dispensing voltage decreases at higher gap heights. It is possible that the higher gap heights (<200 μm) used in this experiment form a more favorable aspect ratio (d/L) for the dispensing operation. (A short movie is available in the supplementary materials: Dispensing Volume Control_03).

3.2.3. Small droplet actuating and splitting

Splitting is a critical step for concentration modification, immunoassay reaction and particle purification [11]. The splitting process requires a strong body force which is related to the tradeoffs among the applied voltage, dielectric material and the hydrophobic surface coating quality. The contact line pinning and CAH of the droplet in the air environment EWOD DMF chips are much more significant than that in a silicone oil environment. Due to the liquid viscosity and the frictions of the droplet-substrate (both top and bottom) interfaces, the droplet splitting slows down or even fails. While doing the splitting experiment, the droplet is stretched by two electrodes until necking [4] appears. Stretching the droplet further results in two sister droplets. However, there can be a problem of open loop splitting. The electrodes at the two ends are competing against each other to drag the droplet forward. Due to the random asymmetrical droplet position, the sister droplet with a larger footprint area (the position) will experience a larger electrostatic force. In this case, asymmetrical splitting may occur. So the success of splitting also depends on the initial position of the droplet. Fast feedback capacitive sensing or an image processing controlled system may help balance the droplet position during the splitting experiment. Asymmetrical droplet position can result in a failed splitting operation when the droplet is small and the gap height is large. Maximum gap heights for splitting droplets ranging from 1.4 μl to 2.0 μl are investigated (Fig. 11a) in this study.

The minimum gap height is set by a tape as the spacer (50 μm). The PZT plate is carefully attached onto the top plate at one end and fixed onto the bonding posts at the other end. This is the 50 μm displacement point that should be calibrated with the laser displacement sensor. The liquid is added to the big reservoirs externally from the left and the right edges of the chip using a pipette without moving the top plate. The smallest droplet that can be dispensed from the reservoir is around 0.1 μl at the lowest gap height (50 μm). Double the gap height, the theoretical dispensed droplet volume is doubled as well.

When the to-be-split droplet is ready on the DMF chip, it is settled in the middle of an electrode and the left and right boundaries should overlap with the neighboring electrodes. First, the gap height is adjusted to a reasonable level for the splitting. If the splitting operation failed, then lower the gap height by 10 μm; if the splitting succeeded, then increase the gap height by 10 μm and try to split it again. To simplify this experiment, we have the splitting electrodes controlled by three external buttons so we can control the splitting and actuation and complete the test quickly. Since we found out low voltages require a longer time to split a droplet during the experiment, we tested the droplet splitting time with different voltages (185–271 V_{RMS}) and different gap heights. The splitting time was recorded.

The droplet shown in Fig. 11(c1–c4) is small relative to the gap height (200 μm) for a proper split operation. After experiencing forces from each electrode the droplet is actuated by electrode '1' rather than split by electrode '1' and '2'. The reason of this failure is that the gap height is too large for the droplet and the footprint areas on the split electrodes (electrode '1' and electrode '2') are too small to be balanced. Decreasing the gap height can increase the footprint areas on electrode '1' and '2'. With a larger footprint area, the droplet is split successfully (Fig. 11(d1–d4), a short movie is available in the supplementary materials: Splitting Small Droplets_04).

A droplet in a certain volume can be split with multiple gap heights. However, larger gap heights may increase the splitting time. Increasing the applied splitting voltage may expedite the splitting process. A 1.5 μl droplet is tested for the splitting time with various applied voltages (Fig. 11(b)). For a 100 μm gap height, using 271 V_{RMS} can save the splitting time for more than 3 s than using 185 V_{RMS}. Using larger voltages for splitting can guarantee efficient splitting operations.

3.3. The portability and the vibration limitations of the proposed DMF system

Compared to the conventional DMF peripheral hardware, the bench equipment such as the function generator and the high power voltage amplifier are avoided in this proposed DMF system. Instead, a portable MOSFET array is integrated into the control circuit. Other peripheral hardware such as the first and the second stage amplifiers, and ADC/DACs are all integrated circuits (IC chips) which are small in size. The system structure shown in Fig. 1 shows the modular design of the DMF control system. All the modules are simply integrated into PCB boards. The laser sensor is integrated in a 1.5 by 3 inches box (the manufactural design), which can be easily mounted to a fixture above the DMF chip. The DMF chip and the operated liquid can be accessible without touching the PZT mounted top plate once it is well calibrated. For the next generation, the system can be improved by adding a flexible microscopic stage and integrating all the hardware into a portable box.

There are some limitations about the vibration amplitude. It was reported that the voltage applied to the electrode makes the

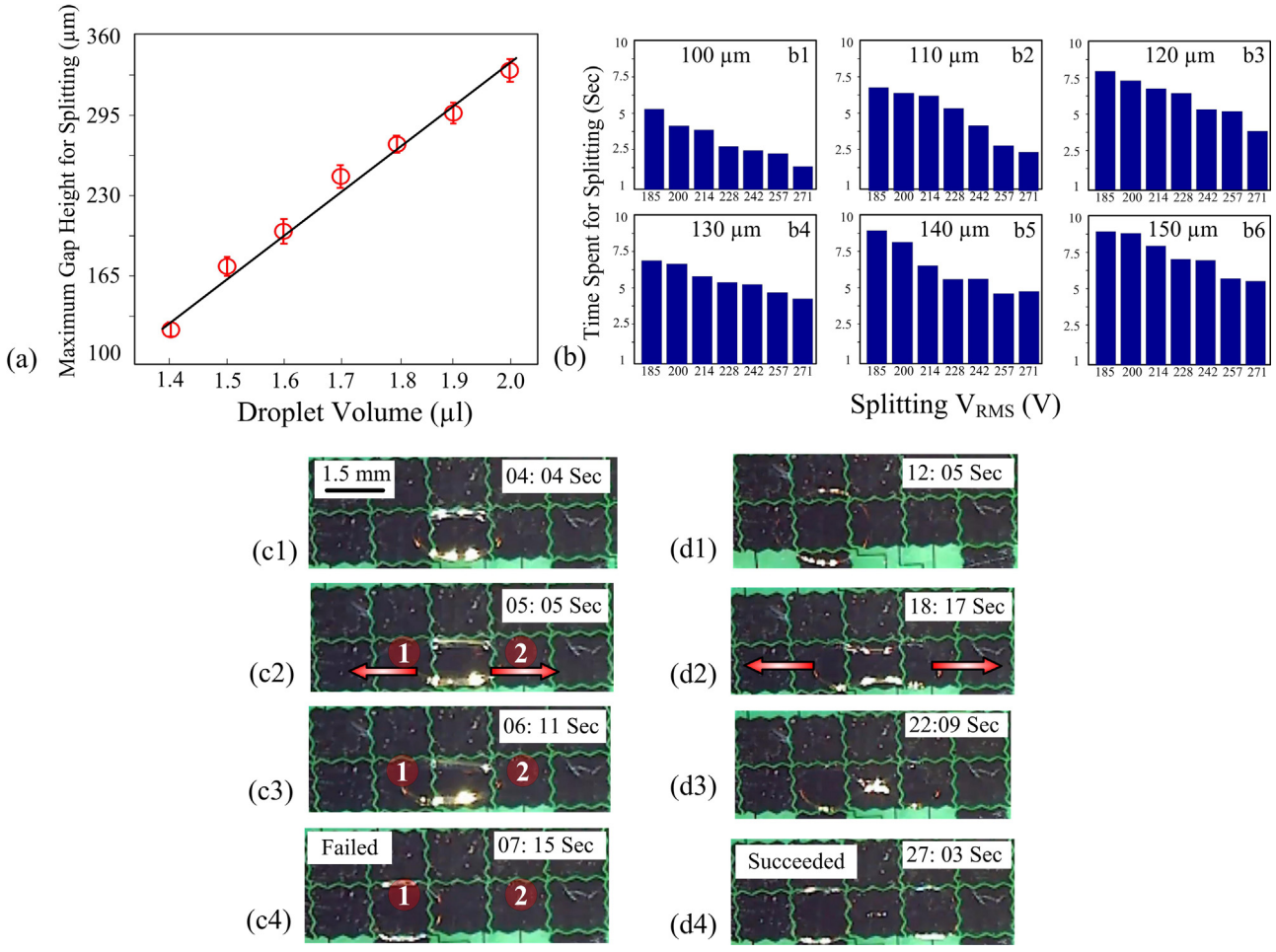

Fig. 11. (a) The largest splitting gap heights for the droplets ranging from 1.4 μl to 2.0 μl. (b) Various applied splitting voltages and their time spent for splitting a 1.5 μl droplet at 100–150 μm gap height. (c1–c4) It failed to split a 1.5 μl droplet at 200 μm gap height. (d1–d4) It succeeded to split the same 1.5 μl droplet at 75 μm gap height. (A short movie is available in the supplementary materials: Splitting Small Droplets_04).

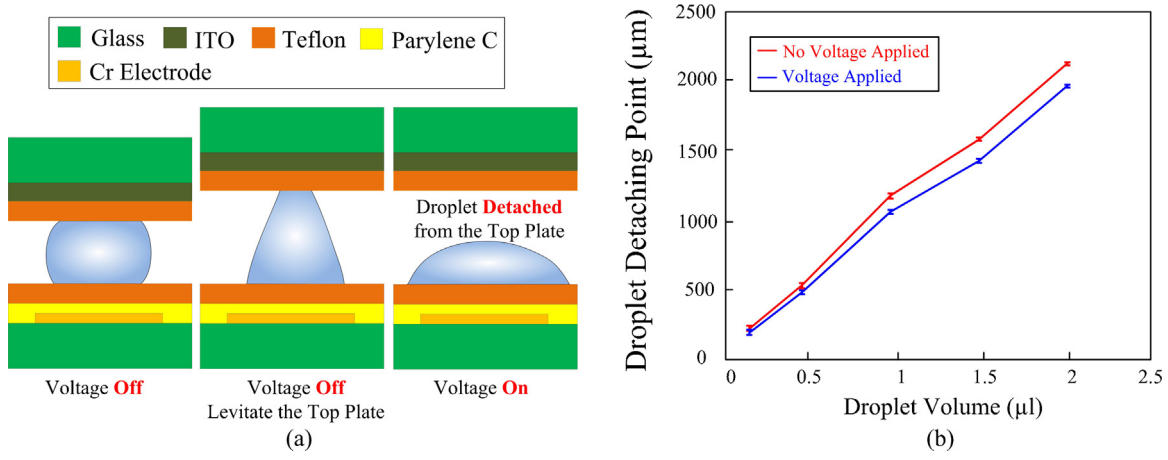

Fig. 12. (a) The top plate vibration has limitations in amplitude to avoid the droplet detaching from the top plate. The droplet spreads on the surface when there is a voltage applied, if the gap height is large, the bridge between the droplet and the top plate will be broken and the droplet will be detached from the top plate. (b) Droplet detaching point with/without an electrowetting voltage.

Teflon coated hydrophobic surface more wettable and indirectly holds the droplet downwards and detaches the droplet from the top plate [63]. The electrowetting-induced detachment happens when the top plate height is comparable to, or higher than the droplet pitch. We tested the droplet detachment in our EWOD system with different droplet volumes, which indicates the top plate vibration amplitude limitations in the future applications (Fig. 12). 250 V_{RMS} voltage pulses are used for the detachment test. The detachment gap height in Fig. 12(b) shows the detaching point with and without a voltage applied to the electrode. The droplet under electrowetting has a lower detaching point. In the regular top plate vibration operations in this study, the gap

height and vibration amplitude is much lower than the vibration limit presented in Fig. 12. For example, for a 0.5 μl droplet, the detachment happens at >500 μm, but the largest possible gap height with vibration is 300 μm in our study (limited by the PZT material). High gap height lowers the aspect ratio of the droplet which impacts on the actuation velocity. So there is no motivation for the user to apply "large" vibration amplitude to the top plate.

4. Conclusion

A new intelligent EWOD DMF top plates mounting technique is proposed and tested in this study. Through gap height control, dispensing volume can be modified in real time. Compared to other micro liquids sensing and actuating techniques such as substrate vibration and SAWs, the top plate vibration technique is compatible with digital controlled EWOD microfluidic chips. The droplet actuation velocity can be sped up to 3 times faster than using static top plates when the driving voltage is insufficient. Much lower threshold actuation voltage is achieved by using a vibrating top plate. With the dynamic control of the top plate, the droplet actuation in the air-filled EWOD DMF chips is more reliable, therefore no oil environment is needed for the real point-of-care diagnostics, which makes the EWOD DMF chips more practical for clinical applications.

Future work can focus on extending the techniques for high throughput automated micro droplet dispensing and transportation. Droplet volume can be tested by embedding a capacitive sensor in the system. The top plate height can then be automatically set depending on the droplet volume. Top plate vibrations and gap height control efficiently optimize the droplet operations without introducing any nano-fabrication processes. By introducing mechanical vibrations, precise positioning of the top plate and capacitive sensing for feedback control into DMF, clinical point-of-care applications using EWOD DMF can be more accurate and useful.

Acknowledgments

We appreciate the helpful discussions with Dr. Ng at University of Toronto, Dr. Guoming Xie at Chongqing Medical University, Dr. Jing Chen at Northeastern University.

Appendix A. Supplementary data

Supplementary data associated with this article can be found, in the online version, at http://dx.doi.org/10.1016/j.snb.2016.01.108.

References

[1] A.H. Ng, B.B. Li, M.D. Chamberlain, A.R. Wheeler, Digital microfluidic cell culture, Annu. Rev. Biomed. Eng. 17 (2015) 1–12.
[2] W.C. Nelson, C. 'Kim, Droplet actuation by electrowetting-on-dielectric (EWOD): a review, J. Adhes. Sci. Technol. 26 (2012) 1747–1771.
[3] P. Paik, V.K. Pamula, R.B. Fair, Rapid droplet mixers for digital microfluidic systems, Lab Chip 3 (2003) 253–259.
[4] S.K. Cho, H. Moon, C. Kim, Creating, transporting, cutting, and merging liquid droplets by electrowetting-based actuation for digital microfluidic circuits, J. Microelectromech. Syst. 12 (2003) 70–80.
[5] Y. Li, H. Li, R.J. Baker, A low-cost and high-resolution droplet position detector for an intelligent electrowetting on dielectric device, J. Lab. Autom. 20 (2015) 663–669.
[6] H. Ren, R.B. Fair, M.G. Pollack, Automated on-chip droplet dispensing with volume control by electro-wetting actuation and capacitance metering, Sens. Actuators B: Chem. 98 (2004) 319–327.
[7] M.A. Murran, H. Najjaran, Capacitance-based droplet position estimator for digital microfluidic devices, Lab Chip 12 (2012) 2053–2059.
[8] Y. Li, H. Li, R.J. Baker, Volume and concentration identification by using an electrowetting on dielectric device, IEEE Dallas Circuits and Systems Conference (2014) 1–4.
[9] M. Schertzer, R. Ben-Mrad, P.E. Sullivan, Using capacitance measurements in EWOD devices to identify fluid composition and control droplet mixing, Sens. Actuators B: Chem. 145 (2010) 340–347.
[10] J. Gong, All-electronic droplet generation on-chip with real-time feedback control for EWOD digital microfluidics, Lab Chip 8 (2008) 898–906.
[11] A.H. Ng, K. Choi, R.P. Luoma, J.M. Robinson, A.R. Wheeler, Digital microfluidic magnetic separation for particle-based immunoassays, Anal. Chem. 84 (2012) 8805–8812.
[12] A.H. Ng, M. Lee, K. Choi, A.T. Fischer, J.M. Robinson, A.R. Wheeler, Digital microfluidic platform for the detection of rubella infection and immunity: a proof of concept, Clin. Chem. 61 (2015) 420–429.
[13] Y. Li, R. Chen, R.J. Baker, A fast fabricating electro-wetting platform to implement large droplet manipulation, IEEE 57th International Midwest Symposium on Circuits and Systems (2014) 326–329.
[14] M. Abdelgawad, A.R. Wheeler, Low-cost, rapid-prototyping of digital microfluidics devices, Microfluid. Nanofluid. 4 (2008) 349–355.
[15] M. Abdelgawad, A.R. Wheeler, Rapid prototyping in copper substrates for digital microfluidics, Adv. Mater. 19 (2007) 133–137.
[16] A.E. Kirby, A.R. Wheeler, Microfluidic origami: a new device format for in-line reaction monitoring by nanoelectrospray ionization mass spectrometry, Lab Chip 13 (2013) 2533–2540.
[17] R. Fobel, A.E. Kirby, A.H. Ng, R.R. Farnood, A.R. Wheeler, Paper microfluidics goes digital, Adv. Mater. 26 (2014) 2838–2843.
[18] A.H. Ng, U. Uddayasankar, A.R. Wheeler, Immunoassays in microfluidic systems, Anal. Bioanal. Chem. 397 (2010) 991–1007.
[19] H. Moon, S.K. Cho, R.L. Garrell, Low voltage electrowetting-on-dielectric, J. Appl. Phys. 92 (2002) 4080–4087.
[20] Y. Lin, R.D. Evans, E. Welch, B. Hsu, A.C. Madison, R.B. Fair, Low voltage electrowetting-on-dielectric platform using multi-layer insulators, Sens. Actuators B: Chem. 150 (2010) 465–470.
[21] M. Pollack, A. Shenderov, R. Fair, Electrowetting-based actuation of droplets for integrated microfluidics, Lab Chip 2 (2002) 96–101.
[22] M.G. Pollack, R.B. Fair, A.D. Shenderov, Electrowetting-based actuation of liquid droplets for microfluidic applications, Appl. Phys. Lett. 77 (2000) 1725–1726.
[23] C.G. Cooney, C. Chen, M.R. Emerling, A. Nadim, J.D. Sterling, Electrowetting droplet microfluidics on a single planar surface, Microfluid. Nanofluid. 2 (2006) 435–446.
[24] J. Berthier, P. Dubois, P. Clementz, P. Claustre, C. Peponnet, Y. Fouillet, Actuation potentials and capillary forces in electrowetting based microsystems, Sens. Actuators A: Phys. 134 (2007) 471–479.
[25] A.N. Banerjee, S. Qian, S.W. Joo, High-speed droplet actuation on single-plate electrode arrays, J. Colloid Interface Sci. 362 (2011) 567–574.
[26] D. Brassard, L. Malic, F. Normandin, M. Tabrizian, T. Veres, Water-oil core-shell droplets for electrowetting-based digital microfluidic devices, Lab Chip 8 (2008) 1342–1349.
[27] J. Hong, Y.K. Kim, K.H. Kang, J.M. Oh, I.S. Kang, Effects of drop size and viscosity on spreading dynamics in DC electrowetting, Langmuir 29 (2013) 9118–9125.
[28] B. Koo, C. Kim, Evaluation of repeated electrowetting on three different fluoropolymer top coatings, J. Micromech. Microeng. 23 (2013) 067002.
[29] M.A. Murran, H. Najjaran, Direct current pulse train actuation to enhance droplet control in digital microfluidics, Appl. Phys. Lett. 101 (2012) 144102.
[30] T. Chen, C. Dong, J. Gao, Y. Jia, P. Mak, M. Vai, R.P. Martins, Natural discharge after pulse and cooperative electrodes to enhance droplet velocity in digital microfluidics, AIP Adv. 4 (2014) 047129.
[31] C. Dong, T. Chen, J. Gao, Y. Jia, P. Mak, M. Vai, R.P. Martins, On the droplet velocity and electrode lifetime of digital microfluidics: voltage actuation techniques and comparison, Microfluid. Nanofluid. (2014) 1–11.
[32] A. DeVoria, K. Mohseni, Droplets in an axisymmetric microtube: Effects of aspect ratio and fluid interfaces, Phys. Fluids (1994-present) 27 (2015) 012002.
[33] M. Yafia, H. Najjaran, High precision control of gap height for enhancing principal digital microfluidics operations, Sens. Actuators B: Chem. 186 (2013) 343–352.
[34] C. Chen, S. Tsai, M. Chen, L. Jang, Effects of gap height, applied frequency, and fluid conductivity on minimum actuation voltage of electrowetting-on-dielectric and liquid dielectrophoresis, Sens. Actuators B: Chem 159 (2011) 321–327.
[35] J. Gao, X. Liu, T. Chen, P. Mak, Y. Du, M. Vai, B. Lin, R.P. Martins, An intelligent digital microfluidic system with fuzzy-enhanced feedback for multi-droplet manipulation, Lab Chip 13 (2013) 443–451.
[36] P. Cruz, A. Mari, P. Roca, Nonlinear time-dependent analysis of segmentally constructed structures, J. Struct. Eng. 124 (1998) 278–287.
[37] O.S. Salawu, C. Williams, Bridge assessment using forced-vibration testing, J. Struct. Eng. 121 (1995) 161–173.
[38] L. Beaulieu, M. Godin, O. Laroche, V. Tabard-Cossa, P. Grütter, A complete analysis of the laser beam deflection systems used in cantilever-based systems, Ultramicroscopy 107 (2007) 422–430.
[39] C. Kranz, G. Friedbacher, B. Mizaikoff, A. Lugstein, J. Smoliner, E. Bertagnolli, Integrating an ultramicroelectrode in an AFM cantilever: combined technology for enhanced information, Anal. Chem. 73 (2001) 2491–2500.
[40] D. Walters, J. Cleveland, N. Thomson, P. Hansma, M. Wendman, G. Gurley, V. Elings, Short cantilevers for atomic force microscopy, Rev. Sci. Instrum. 67 (1996) 3583–3590.

[41] M. Fairbairn, S. Moheimani, Sensorless enhancement of an atomic force microscope micro-cantilever quality factor using piezoelectric shunt control, Rev. Sci. Instrum. 84 (2013) 053706.
[42] R. Borcia, I.D. Borcia, M. Bestehorn, Can vibrations control drop motion? Langmuir 30 (2014) 14113–14117.
[43] L. Rayleigh, On the capillary phenomena of jets, Proc. R. Soc. London 29 (1879) 71–97.
[44] M. Alvarez, J. Friend, L.Y. Yeo, Rapid generation of protein aerosols and nanoparticles via surface acoustic wave atomization, Nanotechnology 19 (2008) 455103.
[45] M. Alvarez, L.Y. Yeo, J.R. Friend, M. Jamriska, Rapid production of protein-loaded biodegradable microparticles using surface acoustic waves, Biomicrofluidics 3 (2009) 014102.
[46] P. Bhattacharjee, A. McDonnell, R. Prabhakar, L. Yeo, J. Friend, Extensional flow of low-viscosity fluids in capillary bridges formed by pulsed surface acoustic wave jetting, New J. Phys. 13 (2011) 023005.
[47] J.R. Friend, L.Y. Yeo, D.R. Arifin, A. Mechler, Evaporative self-assembly assisted synthesis of polymeric nanoparticles by surface acoustic wave atomization, Nanotechnology 19 (2008) 145301.
[48] J. Friend, L.Y. Yeo, Microscale acoustofluidics: microfluidics driven via acoustics and ultrasonics, Rev. Mod. Phys. 83 (2011) 647.
[49] R.P. Hodgson, M. Tan, L. Yeo, J. Friend, Transmitting high power rf acoustic radiation via fluid couplants into superstrates for microfluidics, Appl. Phys. Lett. 94 (2009) 024102.
[50] H. Li, J. Friend, L. Yeo, A. Dasvarma, K. Traianedes, Effect of surface acoustic waves on the viability, proliferation and differentiation of primary osteoblast-like cells, Biomicrofluidics 3 (2009) 034102.
[51] L.Y. Yeo, J.R. Friend, Ultrafast microfluidics using surface acoustic waves, Biomicrofluidics 3 (2009) 012002.
[52] L.Y. Yeo, J.R. Friend, Surface acoustic wave microfluidics, Annu. Rev. Fluid Mech. 46 (2014) 379–406.
[53] S. Daniel, S. Sircar, J. Gliem, M.K. Chaudhury, Ratcheting motion of liquid drops on gradient surfaces, Langmuir 20 (2004) 4085–4092.
[54] A. Quinn, R. Sedev, J. Ralston, Influence of the electrical double layer in electrowetting, J. Phys. Chem. B 107 (2003) 1163–1169.
[55] http://cmosedu.com/cmos1/electric/electric.htm.
[56] X. Zhao, Y. Tan, Neural network based identification of Preisach-type hysteresis in piezoelectric actuator using hysteretic operator, Sens. Actuators A: Phys. 126 (2006) 306–311.
[57] G. Robert, D. Damjanovic, N. Setter, A. Turik, Preisach modeling of piezoelectric nonlinearity in ferroelectric ceramics, J. Appl. Phys. 89 (2001) 5067–5074.
[58] J.E. Longley, E. Dooley, D.M. Givler, W.J. Napier III, M.K. Chaudhury, S. Daniel, Drop motion induced by repeated stretching and relaxation on a gradient surface with hysteresis, Langmuir 28 (2012) 13912–13918.
[59] C. Chang, J.B. Bostwick, P.H. Steen, S. Daniel, Substrate constraint modifies the Rayleigh spectrum of vibrating sessile drops, Phys. Rev. E 88 (2013) 023015.
[60] H.P. Greenspan, On the motion of a small viscous droplet that wets a surface, J. Fluid Mech. 84 (1978) 125–143.
[61] S. Daniel, M.K. Chaudhury, J.C. Chen, Fast drop movements resulting from the phase change on a gradient surface, Science 291 (2001) 633–636.
[62] J. Song, R. Evans, Y. Lin, B. Hsu, R. Fair, A scaling model for electrowetting-on-dielectric microfluidic actuators, Microfluid. Nanofluid. 7 (2009) 75–89.
[63] J. Gong, G. Cha, Y.S. Ju, C. Kim, Thermal switches based on coplanar EWOD for satellite thermal control, IEEE 21st International Conference on Micro Electro Mechanical Systems (2008) 848–851.

Biographies

Yiyan Li received his B.S. degree in biomedical engineering from Henan University of Science and Technology, in 2009, and his M.S. degree in biomedical engineering from Chongqing University, in 2012. He is currently a Ph.D. candidate in electrical and computer engineering at University of Nevada Las Vegas. His research interest includes the development of high throughput automated EWOD DMF chips for immunoassay experiments, nanomaterial fabrication, analog to digital converters and electrical stimulation for neural disorders.

Russel Jacob (Jake) Baker (S'83-M'88-SM'97-F'13) was born in Ogden, Utah, on October 5, 1964. He received the B.S. and M.S. degrees in electrical engineering from the University of Nevada, Las Vegas, in 1986 and 1988. He received the Ph.D. degree in electrical engineering from the University of Nevada, Reno in 1993. From 1981 to 1987 he served in the United States Marine Corps Reserves. From 1985 to 1993 he worked for E. G. & G. Energy Measurements and the Lawrence Livermore National Laboratory designing nuclear diagnostic instrumentation for underground nuclear weapons tests at the Nevada test site. From 1993 to 2000 he served on the faculty in the department of electrical engineering at the University of Idaho. In 2012 he joined the faculty at the University of Nevada, Las Vegas where his research focuses on the design of diagnostic instrumentation for scientific research, integrated electrical/biological circuits and systems, methods to fabricate trusted integrated circuits, array (memory and displays) circuit design, and low-power interconnect techniques, communication circuit design, and the delivery of online engineering education.

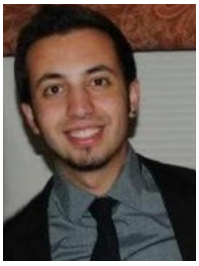

Dominic Raad received his B.S. degree at University of California, Davis in 2011. He is now serving as a senior engineer at Kisco Conformal Coating, LLC. His expert is in chemical vapor deposition, analyzing hazardous materials and process ranked under S.E.M.I. standards, constructing and executing tests for air pattern, toxicity, P.H.A., and other S.E.M.I. S6 methods.